Journal of Hazardous Materials 186 (2011) 1103–1110

Contents lists available at ScienceDirect

Journal of Hazardous Materials

journal homepage: www.elsevier.com/locate/jhazmat

Yttrium and lanthanides in human lung fluids, probing the exposure to atmospheric fallout

P. Censi[a,b,c,*], E. Tamburo[a], S. Speziale[d], P. Zuddas[e], L.A. Randazzo[a,b,c,e], R. Punturo[f], A. Cuttitta[b], P. Aricò[a]

[a] Dipartimento C.F.T.A., Università di Palermo, Via Archirafi, 36 90123 - Palermo, Italy
[b] I.A.M.C.-CNR – UOS di Capo Granitola, Via faro, 1 - 91026 Torretta Granitola, Campobello di Mazara (TP), Italy
[c] En.Bio.Tech. – Via Aquileia, 35 90100 Palermo, Italy
[d] Deutsches GeoForschungsZentrum, Telegrafenberg, Potsdam, 14473, Germany
[e] Institut Génie de l'Environnement et Ecodéveloppement & Département Sciences de la Terre, UMR 5125, Université Claude Bernard Lyon 1, 2 rue R. Dubois, Bat GEODE 69622 Villeurbanne Cedex, France
[f] Dipartimento di Scienze Geologiche, Università di Catania, Corso Italia, 55 - 95129 Catania, Italy

ARTICLE INFO

Article history:
Received 25 May 2010
Received in revised form
26 November 2010
Accepted 26 November 2010
Available online 3 December 2010

Keywords:
Medical geochemistry
Lanthanides
Yttrium
Volcanic ash
Bronchoalveolar lavages
Dendriform pulmonary ossification

ABSTRACT

Inhalation of airborne particles can produce crystallization of phosphatic microcrysts in intraaveolar areas of lungs, sometimes degenerating into pulmonary fibrosis. Results of this study indicate that these pathologies are induced by interactions between lung fluids and inhaled atmospheric dust in people exposed to volcanic dust ejected from Mount Etna in 2001. Here, the lung solid–liquid interaction is evaluated by the distribution of yttrium and lanthanides (YLn) in fluid bronchoalveolar lavages on selected individuals according the classical geochemical approaches. We found that shale-normalised patterns of yttrium and lanthanides have a 'V shaped' feature corresponding to the depletion of elements from Nd to Tb when compared to the variable enrichments of heavy lanthanides, Y, La and Ce. These features and concurrent thermodynamic simulations suggest that phosphate precipitation can occur in lungs due to interactions between volcanic particles and fluids. We propose that patterns of yttrium and lanthanides can represent a viable explanation of some pathology observed in patients after prolonged exposure to atmospheric fallout and are suitable to become a diagnostic parameter of chemical environmental stresses.

1. Introduction

Investigating the effects on human health of the exposure to potentially hazardous geological materials represents one of the present issues in comprehension of the Earth dynamics [1]. The human pulmonary system is a place where inhaled geological particulates material can interact with lung fluid and relative tissues. Dendriform pulmonary ossification (DPO) and pulmonary microlithiasis (PAM) are two rare diseases that have been recognized in the lungs of individuals who have inhaled atmospheric particles released by industrial practices or hydrocarbon combustion [2]. Both these pathologies generate new phosphatic microcrysts in intraaveolar areas of the lungs [3,4] that may progress to pulmonary fibrosis [5]. Both DPO and PAM are considered difficult to recognise under *in vivo* observations, whereas their occurrence is usually evidenced only after authoptic examination.

Causes of these diseases are not well defined, although the disposal of metal dust with large affinity to phosphate precipitation, such as lanthanides, can represent a suitable possibility. This suggestion agrees with recognition of DPO in people exposed to industrial dust produced during the manufacture of mirrors, optical lenses, and certain electronic components that are usually considered lanthanide-rich materials [6–11].

Trace elements present in atmospheric particles of either natural or anthropogenic origin can dissolve in lung fluid [12–14]. Since the phosphate (PO_4^{3-}) concentration in lung fluid is approximately 1.175 mmol l^{-1} [15], some cations with an affinity for phosphate, such as those of the lanthanides, can crystallize in interstitial lung spaces. This can be observed using a mildly invasive procedure in which broncho-alveolar lavage (BAL) fluid is analysed for YLn content using a shale-normalised approach. Techniques borrowed from geochemistry are used to identify dissolved particles and their phosphate crystallizations. This method can be used to assess DPO and PAM induction, and has been texted in human lung fluids of individuals exposed to freshly released volcanic particles by inhalation. This may represent a suitable explaination of DPO and PAM induction and has been tested in human lung fluids of

* Corresponding author at: Dipartimento C.F.T.A., Università di Palermo, Via Archirafi, 36 90123 - Palermo, Italy. Tel.: +39 3479662844; fax: +39 0916168376.
E-mail address: censi@unipa.it (P. Censi).

0304-3894/$ – see front matter © 2010 Elsevier B.V. All rights reserved.
doi:10.1016/j.jhazmat.2010.11.113

people exposed by inhalation of freshly released volcanic particles.

2. Experimental

2.1. Brief characterization of the fine particulates emitted by the eruption of Mount Etna in the summer of 2001

During the eruption of Mount Etna in the summer 2001 the amount of ejecta was so large as to cause the deposition of about 0.39 kg m^{-2} ash between 21 and 24 July 2001 in the area [16]. Volcanic ejecta typically consisted of a mixture of several solids ranging from particles made of silicate minerals and volcanic glass to soluble salts adsorbed onto those particles [17–19]. The solid fraction of ejected materials mainly consisted of glass fragments (about 70%) with smaller amounts of clinopyroxene (about 15%) and minor amounts of olivine and spinel [20,21]. There is a soluble ash fraction (SAF) that coats the solid particles, and it consisted of highly soluble sublimates of acids, metal salts, and adsorbed halogen-rich fluids (formed during the uprising of the volcanic eruptive plume [16].

2.2. BAL extraction and chemical processing of the samples

Six patients in care at the Dipartimento di Medicina Interna e Medicina Specialistica of the Università degli Studi di Catania were subject (after giving their written informed consent) to the BAL procedure during the summer of 2001. This occurred immediately after residents of the city of Catania were exposed by inhalation to volcanic ash produced by pyroclastic activity of Mount Etna, the largest European volcano. Due to the particular location of Catania with respect to the eruptive source and the ambient meteorological conditions, there was an extreme deposition of volcanic particles mainly consisting of mineral, glass and rock fragments between 1 and 500 μm diameter, with main grain-size in the range of 5–10 μm diameter [22,16]. The International Commission on Radiological Protection (ICRP) considers that the percentage of respirable particles within the size range of 5–10 μm is 30–1%, respectively.

BALs were obtained by instillation of four lavages carried out with 30 ml aliquots of physiological solution (SW) using a fibrobronchoscope according to Bargagli et al. [23]. Each aliquot was immediately gently aspirated. From each lavage the first 20 ml of sample were used to clean the fibrobronchoscope and the next 10 ml of sample, after filtration with a 0.22 mm Nalgene™ membrane, were used for chemical investigations. BAL samples were treated with 15 ml of hydrogen peroxide, 5 ml of HNO_3 30% solution, 1.5 ml of HCl 30% solution and 0.1 g of solid NH_4F in a polytetrafluoroethylene (TFM™) reactor. Reactors were sealed and heated in a microwave oven (MARS 5™, CEM Technologies) at 3×10^5 Pa and 200 °C for 30 min. Acid excess was removed from each solution up to incipient dryness using a CEM microvap™ apparatus and HNO_3 solution (5%, v/v) was added to attain final solution volumes of 20 ml. The solutions were finally transferred to previously cleaned polycarbonate vials. The samples were treated under a laminar air flow clean bench to minimize contamination risks.

YLn analyses were carried out with a double focusing magnetic sector field inductively coupled plasma mass spectrometer SF-ICP-MS Thermo-Scientific Element 2, without gas chromatograph, using an external calibration approach. BAL analyses are reported in Table 1. All the investigated elements were analyzed in medium-resolution mode, apart from Y and La that were determined in high-resolution mode, in order to avoid an overestimation of true concentrations due to effects of interferences of polyatomic Ar-

Table 1
YLn contents measured in BAL solutions. The analysed masses and the used resolutions are also reported. nd: not determined.

Person ntificative acronym	Yμg l^{-1}	Laμg l^{-1}	Ceμg l^{-1}	Prμg l^{-1}	Ndμg l^{-1}	Pm μg l^{-1}	Smμg l^{-1}	Euμg l^{-1}	Gdμg l^{-1}	Tbμg l^{-1}	Dyμg l^{-1}	Hoμg l^{-1}	Erμg l^{-1}	Tmμg l^{-1}	Yb v	Luμg l^{-1}
AG	10.215	32.822	11.978	0.253	0.983	nd	0.122	0.0316	0.15	0.02	0.1066	0.0316	0.1067	0.028	0.103	0.019
SC	15.549	93.339	30.962	0.229	0.935	nd	0.118	0.0631	0.206	0.024	0.1255	0.0397	0.1102	0.02	0.118	0.023
BR	18.855	85.56	30.016	0.372	0.321	nd	0.03	0.033	0.165	0.032	0.21	0.032	0.1145	0.021	0.182	0.045
CA	14.776	76.408	31.302	0.427	1.666	nd	0.265	0.1309	0.356	0.028	0.2692	0.0475	0.2019	0.028	0.23	0.039
M	22.701	102.718	38.733	0.218	0.401	nd	0.043	0.017	0.075	0.017	0.1666	0.037	0.0874	0.026	0.123	0.037
RG	15.786	77.637	30.846	0.399	1.55	nd	0.257	0.095	0.32	0.039	0.3206	0.0594	0.2733	0.034	0.313	0.046

bearing species. Although several polyatomic interferences based on Ar-bearing species can influence the correct evaluation of investigated masses, this problem can be avoided using a high-resolution sector field ICP-MS like this used in this research. On the other hand the problem of the over estimation of the mass of interest partially still remains for ^{89}Y which is influenced by $^{49}Ti^{40}Ar$ species also under high resolution mode. According to the Thermo Finnigan Interference Workshop™ this interference can be avoided with 20,000 $M-\Delta M^{-1}$ theoretical resolution that cannot be attained with our SF-ICP-MS. On the other hand a $^{89}Y/^{49}Ti^{40}Ar$ signal-to-noise ratio close to 100 has very limited influence of the correct evaluation of the Y content. Although we did not monitor the ^{49}Ti mass, very low Ti concentrations are expected in BAL samples due to the very low solubility of Ti-bearing materials, both of lithogenic and anthropogenic origin where ^{49}Ti represents only 5.5% of the entire Ti abundance. The calibration for each element was based on 7 standard solutions at known concentrations. Analytical precision was evaluated using the same physiological solution (SW) used for collection of BAL samples, due to the absence of standard reference materials with certified values for all the investigated elements. Five aliquots of SW solution were added with the same quantities of chemicals used for the BAL samples treatment, they were subject to mineralization procedures and then used as procedural blanks (PBs). YLn contents measured in PBs were used to evaluate the critical values (L_C), the detection limits (L_D) and the limit of quantification (L_Q) for the investigated trace elements, according to EPA [24]. Obtained results are reported in Table 2. The low L_Q values indicate that the amounts of trace metals lost and/or added during recovery procedures and sample preparation are negligible with respect to the trace element contents of BAL samples.

All the studied solutions were prepared with Millipore ultrapure water (18.2 MΩ). All used chemicals were Merck ULTRAPUR®. All the materials used to sample and manipulate water samples were plasticware acid cleaned with hot 1:10 HNO_3 solutions.

2.3. Thermodynamic modeling

In order to evaluate if interactions between lung fluids and volcanic particles could induce crystallization of secondary phases, we followed the modeling approach. Modeling calculations were carried out using the composition of simulated lung fluid (SLF) reported by Wood et al. [25], taking in account that SLF dissolves the soluble-ash fraction (SAF) of suspended volcanic particulates after quick reaction. Due to the large SAF solubility the rate of the glass dissolution was supposed to be negligible with respect to the rate of SAF dissolution in lung fluids. As a consequence the SLF composition was modified (simulated modified lung fluid, here called SMLF) before interacting with glass and crystalline fractions of volcanic particles. In our calculations the fractionation of YLn induced by the occurrence of colloidal phase was not considered because the colloidal stability in aquatic systems is limited to low salinity conditions (0–6 mg l^{-1}) [26,27]. On the contrary, salt contents of lung fluids and the physiological solution used for BAL collection (9.5 and 11.4 mg l^{-1}, respectively) were too high to involve the occurrence of a significant colloidal phase in these fluids. YLn contents in SMLF are reported in Table 3. Chemical modifications induced in SMLF by the dissolution of the glassy-ash fraction were evaluated with the aid of the EQ3/6, version 7.2b software package [28–30], using the LLNL thermodynamic database from the Lawrence Livermore National Laboratory, where the same software package was developed. EQ3/6 algorithm models the chemical evolution of geochemical systems using thermodynamic and kinetic constraints. In order to treat rock–water interactions in a lung system leading to major, minor and trace element released, the double solid reactant method (DSRM) was adopted according to Accornero and Marini [31]. This approach is usually carried out to model trace

Table 2
YLn concentrations measured in procedural blanks (PBs) and related critical values (L_C), detection limits (L_D) and limits of quantification (L_Q) for the investigated trace elements. YLn concentrations measured in five repeated analyses of an artificially prepared standard physiological solution having 10 ng l^{-1} nominal concentration of each YLn. nd: not determined.

	Resolution	PB-1 ng l^{-1}	PB-2 ng l^{-1}	PB-3 ng l^{-1}	PB-4 ng l^{-1}	PB-5 ng l^{-1}	L_C ng l^{-1}	L_D ng l^{-1}	L_Q ng l^{-1}	SW-1 ng l^{-1}	SW-2 ng l^{-1}	SW-3 ng l^{-1}	SW-4 ng l^{-1}	SW-5 ng l^{-1}	SW_{mean} ng l^{-1}	$\sigma\pm$ ng l^{-1}
^{89}Y	High	0.92	0.72	1.09	0.62	0.7	0.17	0.34	1.05	8.93	10.44	9.87	10.82	9.51	9.91	0.75
^{139}La	High	0.22	0.18	0.34	0.1	0.16	0.05	0.09	0.29	9.89	9.66	9.55	10.18	9.8	9.82	0.24
^{140}Ce	Medium	0.3	0.47	0.35	0.32	0.46	0.05	0.1	0.32	8.98	9.64	9.01	9.55	9.64	9.36	0.34
$^{141}P_r$	Medium	0.28	0.42	0.35	0.32	0.51	0.09	0.18	0.54	9.35	9.67	9.09	9.87	9.73	9.54	0.32
^{146}Nd	Medium	0.09	0.05	0.12	0.06	0.08	0.02	0.04	0.12	9.74	9.29	9.62	9.46	9.43	9.51	0.17
Pm		nd	nd	nd	nd	nd	nd	nd	nd	nd	nd	nd	nd	nd	nd	nd
^{147}Sm	Medium	0.1	0.08	0.17	0.06	0.09	0.03	0.06	0.19	9.81	9.43	9.46	9.83	9.29	9.56	0.24
^{151}Eu	Medium	0.1	0.13	0.22	0.14	0.14	0.02	0.04	0.11	10.03	10.17	10.02	9.25	9.08	9.71	0.5
^{157}Gd	Medium	0.18	0.16	0.33	0.21	0.22	0.04	0.08	0.24	10.53	9.42	10.16	9.97	9.18	9.85	0.55
^{159}Tb	Medium	0.29	0.55	0.49	0.39	0.6	0.03	0.06	0.19	11.05	9.68	9.51	9.93	9.49	9.93	0.65
^{163}Dy	Medium	0.35	0.57	0.4	0.33	0.58	0.09	0.18	0.56	9.19	10.13	9.52	9.36	9.73	9.59	0.37
^{165}Ho	High	0.34	0.5	0.43	0.39	0.51	0.02	0.04	0.14	9.65	9.9	11.72	9.37	9.6	10.05	0.95
^{166}Er	High	0.32	0.52	0.45	0.33	0.51	0.07	0.15	0.46	9.28	11.6	11.03	11.09	10.18	10.63	0.91
^{169}Tm	High	0.29	0.6	0.46	0.36	0.64	0.07	0.14	0.44	8.91	9.42	10.07	9.43	11.03	9.77	0.82
^{172}Yb	High	0.3	0.58	0.53	0.37	0.51	0.03	0.07	0.21	9.39	9.55	11.4	9.27	10.47	10.02	0.91
^{175}Lu	High	0.38	0.56	0.54	0.36	0.61	0.08	0.17	0.52	10.21	10.58	11.08	9.81	10.08	10.35	0.49

Table 3
YLn contents modeled in simulated modified lung fluids (SMLF) after dissolution of soluble-ash fraction, immediately before to crystallization of YLn-phosphates $[YLn]_0$. nd: not determined.

	Y $\mu g l^{-1}$	La $\mu g l^{-1}$	Ce $\mu g l^{-1}$	Pr $\mu g l^{-1}$	Nd $\mu g l^{-1}$	Pm $\mu g l^{-1}$	Sm $\mu g l^{-1}$	Eu $\mu g l^{-1}$	Gd $\mu g l^{-1}$	Tb $\mu g l^{-1}$	Dy $\mu g l^{-1}$	Ho $\mu g l^{-1}$	Er $\mu g l^{-1}$	Tm $\mu g l^{-1}$	Yb $\mu g l^{-1}$	Lu $\mu g l^{-1}$
SMLF	0.003	0.007	0.01	nd	0.006	nd	0.001	0.0005	0.001		0.0003	0.0001	0.0003	0.004	0.001	0.004
$[YREE]_0$	12.2	41.9	64.1	nd	24.3	nd	518	2.36	3.75		2.43	0.43	1.09	0.16	0.97	0.15

Table 4
List of the parameters in the thermodynamic modeling.

Parameter symbol	Description	Units
$N_{+,ij}$	Mechanism-specific reaction order	
$n_{T+,ij}$	Activity of aqueous species number ($iT+,j$) of parallel mechanisms, each one comprising a rate constant ($k+,ij$), a kinetic activity product, and a term	
i	Depending on thermodynamic affinity ($A+,j$)	
r_ϕ	Dissolution rate	$mol\,s^{-1}$
A_{Sj}	Physical surface area of jth solid	cm^2
f_j	Ratio of reactive to physical surface area	
$k_{+,ij}$	Kinetic rate constant	$mol\,cm^{-2}\,s^{-1}$
a_n	Term depending on thermodynamic affinity	
$\sigma_{+,ij}$	Temkin's coefficient	
T	Absolute temperature	K
A_{+j}	Thermodynamic affinity of jth solid	
R	Gas constant	$J\,mol^{-1}\,K^{-1}$

elements released to the aqueous solution during dissolution of host rocks. In fact, thermodynamic models and rate laws based on transition state theory (TST) [32,33] can be used to describe trace elements release during dissolutions of primary minerals. In DSRM, each dissolving solid phase is considered as a double solid reactant, consisting of a pure mineral or a solid mixture (*the solid reactant*) and another reactant, defined as the *special reactant* according to EQ6 nomenclature. Basaltic glass is considered to be a mixture of amorphous silica and cryptocrystalline AlOOH; therefore, the hydrolysis reaction for amorphous silica and gibbsite, rather than for crystalline silica, was used to better simulate natural conditions [34]. Thermodynamic and kinetic properties of the solid reactant are enclosed in the geochemical database and determine analogous properties (i.e. equilibrium constant of the hydrolysis reaction), whereas the same features are unknown for the special reactant. The saturation state of the aqueous solution with respect to the solid reactant is calculated during the progressive dissolution of rocks until the attainment of the solution saturation.

The input parameters utilized in EQ 6 thermodynamic model for dissolution of volcanic particle components by lung fluids include: (a) composition and surface area of solid reactant, (b) the speciation model consistent with the composition of SMLF and (c) kinetic parameters of the solid reactant. The first two parameters are obtained from analyses of solid and liquid reactants and construction of the speciation model with the aid of the EQ3NR computer code. Reaction path modeling has been carried out according to a kinetic approach based on the TST. Rate-laws are written in the form [35]:

$$r_\varphi = f_i A_{Sj} \sum_{i=1}^{i_{T+j}} k_{+,ij} \left(\prod_{n=1}^{n_{T+ij}} a_n^{-N_{+ij}} \right) (1 - e^{-(A_{+j}/\sigma_{+ij}RT)}) \quad (1)$$

The terms in brackets are the kinetic activity product taking into account the effect of the dissolved composition and the affinity factor that is influenced by the distance from equilibrium. Symbols used in Eq. (1) are explained in Table 4.

The reaction progress is described by the variable ξ (expressed in moles) that measures the relative extent of the reactive process [35–37]. In EQ6, reaction progress variables are used to describe only the reactions that are irreversible (not at equilibrium). The irreversible process is defined by an array of simple irreversible reactions. A reaction progress (ξ) is associated to each of these reactions. There is in addition an overall reaction progress variable (ξ) for the process as a whole. The investigated system consists of a primary mineral, an aqueous solution and

other secondary minerals that can crystallize as a consequence of solid–liquid interactions. The reaction path modeling starts taking into account the dissolution of basaltic glass according to the reaction

$$SiAl_{0.36}O_2(OH)_{1.08} + 0.36H_2O = SiO_2 + 0.36Al(OH)_4^- + 0.36H^+.$$

Thermodynamic properties were estimated from the stoichiometrically weighted sum of hydrolysis reactions for amorphous silica and gibbsite. They were re-computed at the temperature, pressure grid required by software package EQ3/6 and included in the thermodynamic database. The kinetic parameters used in this simulation correspond to the Gislason and Oelkers estimations [34]. Inhaled particles interesting the deep lung area should have diameters lower than 3 μm [38]. Their shape was suggested by optical observations carried out on the material used for kinetic experiments and revealed wide presence of glass with low porosity and rounded, rather than irregular shape. Therefore we did not measure the specific surface area of these products with a BET approach, according to Wolff-Boenisch et al. [39] who reported that dissolution rates of volcanic glass particles were more closely proportional to geometric surface area rather than their BET surface area. Thus the geometrical surface area of ash was calculated assuming a spherical grain shape (with radius equal to 0.3 μm) with intra-grain porosity equal to 0.3. Although this can be considered an arbitrary choice and a scalene ellipsoidal form could be more adequate to describe features of ash grains [40], recent investigations suggest that real ash particles have higher surface areas that geometric forms due to their roughness [41] and the geometrical approach attains to minimum surface area values. On the other hand Ersoy's results corroborate our choice of a spherical shape of grains in volcanic product because indicate that the spherical assumption of ash shape better than the ellipsoidal form simulates the surface area/volume ratio of natural products, especially for the finest grain size. Clearly, modeling the interface area according to a geometric approach rather than its direct assessment induces an underestimation of interacting solid–liquid surface and consequently involves an incorrect evaluation of leaching rate of investigated elements. On the other hand the reactivity of volcanic ash in lungs is taking in account only in terms of reaction progress (ξ), not in terms of absolute time, to assess if the modeling approach attains to results that corroborate geochemical indications of crystallization of lanthanide phosphate. Trace element concentrations were used to define a special reactant associated with hydrated basaltic glass in DSRM. Model calculations were performed under open-system conditions (being the system in contact with a large external gas reservoir) at 37 °C (body temperature). Simulated physical-chemical conditions, major and minor elemental concentrations in SMLF are reported in Table 5. In the reaction path modeling, a set of realistic secondary solid phases has been allowed to precipitate, including the minerals which have been shown to reach saturation at the investigated conditions, and alteration minerals originated from hydrated basaltic glass (gibbsite, kaolinite, chalcedony, saponite and a mechanical mixture of transition metal hydroxides, constituted by ferrihydrite, $Fe(OH)_2$, $Cr(OH)_3$, $Mn(OH)_3$, amorphous $Mn(OH)_2$, $Co(OH)_2$, $Ni(OH)_2$, $Cu(OH)_2$, and ε-$Zn(OH)_2$). Instantaneous equilibrium between these minerals and lung fluids was assumed. As regards to YLn, the composition of lung fluids, usually mirrored by Gamble's solution [15], implied that the most suitable lanthanides precipitating phase was the phosphate and this hypothesis also agreed with model calculations carried out by Wood et al. [25]. However, YLn do not form pure phosphates [42]. Instead, due to the close similarities in their ionic radii the entire YLn suite in presence of PO_4^{3-} in natural solutions forms coprecipitates [42]. YLn compositions is related to the composition of parent solution (pf) according to the relation-

Table 5
Major and minor element contents, pH and fCO_2 used in SMLF for thermodynamic modeling. Model simulations were carried out at 37 °C. Set values are consistent with those occurring in lung fluids.

pH	Al μg l^{-1}	Ca μg l^{-1}	Mg μg l^{-1}	Fe μg l^{-1}	Mn μg l^{-1}	Na μg l^{-1}	K μg l^{-1}	Cl μg l^{-1}	F μg l^{-1}	SO_4^{2-} μg l^{-1}	$Ti(OH)_4$(aq) μg l^{-1}	SiO_2(aq) μg l^{-1}	HPO_4^{2-} μg l^{-1}	fCO_2 Pa
7.4	34	6	0.2	0.01	1	5	0.01	80	3	680	0.01	10	20	500

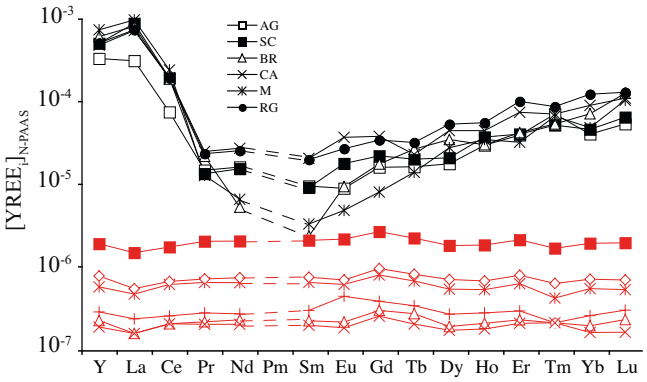

Fig. 1. Shale-normalised YLn contents in BAL fluids (black symbols). Concentrations of soluble-ash fractions from Etna [50] are reported as reference (red symbols). (For interpretation of the references to color in this figure legend, the reader is referred to the web version of the article.)

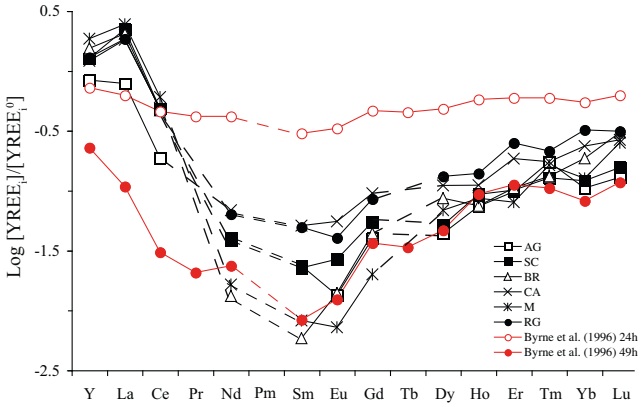

Fig. 2. YLN fractionation calculated between initial modeled concentrations of SMLF and BAL solutions. For further details see text. YLn fractionations induced by crystallization of YLn-phosphate after 24-h and 49-h [43] are reported for comparison.

ship:

$$\left(\frac{YLn_i}{YLn_j}\right)_{PO_4^{3-}} = \lambda_{ij}\left(\frac{YLn_i}{YLn_j}\right)_{pf} \quad (2)$$

where $[YLn_i]$ and $[YLn_j]$ denote concentrations of two elements of the suite in co-precipitates (PO_4^{3-} subscript) and coexisting fluid (pf subscript), respectively, whereas λ_{ij} are factors that influence the relative YLN fractionations. Therefore, being coexisting fluid represented by SMLF, on the basis of λ_{ij} values measured by Byrne et al. [43] the consisting YLn concentrations in the hypothetical co-precipitated phosphate were calculated. The YLn-phosphate concentration in agreement with SMLF data and λ_{ij} values is $Y_{0.15}La_{0.15}Ce_{0.31}Nd_{0.24}Sm_{0.10}Gd_{0.05}(PO_4)$. This chemical composition to falls in the range of monazites, a common natural phosphate mineral [44] thus, the thermodynamic properties of natural monazite were used during the calculation. During simulations, newly-formed authigenic minerals are considered isolated with respect to the residual lung fluid and do not react with it.

3. Results

YLn cumulative concentrations in the BAL samples analyzed in this study span a range from 56.9 to 165.4 $\mu g\,l^{-1}$. However, the relative abundances of the different elements in the REE series plus Y are all very similar in all the samples, with Y and light REE (LREE), La, Ce and Pr, as the most abundant elements. The overall pattern of YLn abundances in BALs are very different with respect to those of the solid components of volcanic ejecta making it unlikely that the wide range of cumulative YLn contents is caused by residual undissolved inhaled volcanic particles (<6.4 μm, [45]) mechanically removed from bronchial tissues during BAL lavages.

Comparing shale-normalised YLn patterns of BAL solutions with analogous patterns for SAF, we observe significant differences (Fig. 1). While the YLn patterns of SAF are flat, those from BAL lavages are flat only between Pr and Eu. Y and La normalised concentrations are about 50 times higher, whereas Ce is about 4 time higher than Pr–Eu normalised concentrations. Normalised concentrations of heavier elements, from Gd to Lu, progressively increase respect to those measured in Pr–Eu interval, attaining to a Lu enrichment of about 3 times. Furthermore, all YLn concentrations are higher in BALs than in SAF.

Since over-estimation of true concentrations, due to spectral interferences, were avoided by measurements carried out both in high and medium resolution modes for the entire suite of investigated elements, the observed enrichments from Y to Nd can be influenced by co-precipitation of YLn-phosphate from lung fluids in intra-alveolar spaces. Indeed features observed in BAL patterns are very similar to those recognised in solutions that experienced YLn-phosphate co-precipitation [43]. As proposed by Byrne and Kim [42], the co-precipitation of trace elements may follow the relationship:

$$\log\left\{\frac{[YLn_i]}{[YLn_i]_0}\right\} = \lambda_{ij}\log\left\{\frac{[YLn_j]}{[YLn_j]_0}\right\} \quad (3)$$

where $[YLn_i]$ and $[YLn_j]$ denote dissolved concentrations during co-precipitation whereas $[YLn_i]_0$ and $[YLn_j]_0$ are the initial concentrations.

In Fig. 2 the behavior of $\log\{[YLn_i]/[YLn_i]_0\}$ values computed for BAL lavages using SMLF as representative of initial concentrations are compared with fractionation patterns determined by Byrne et al. [43] in a study of YLN fractionation during phosphates co-precipitation from solutions at 25 °C and pH ≈ 4 between 24 and 49 h. Patterns relative to BAL solutions are similar to 49 h phosphate co-precipitation pattern, rather than after 24 h [43]. This suggests that phosphate co-precipitation had different amplitude in studied individuals probably as a consequence of different amount of inhaled atmospheric dust. Therefore, if the particle dissolution occurred during a longer time, phosphate co-precipitation had a longer duration and YLn were more intensely fractionated. Since $\log\{[YLn_i]/[YLn_i]_0\}$ BAL values for Y, La and Ce in Fig. 2 are often higher than those in phosphate co-precipitation [43], the concurrent presence of an additional particulates source of these elements cannot be excluded (i.e. anthropogenic particulates, [46]).

The recognition of newly-formed phases in lungs usually requires micrometric scale observations that need to remove lung tissues by biopsy [4,11]. This is particularly expensive and not easily made in routine hospital practice in many countries. The results of our calculations indicate that effectively the SMLF-ash interaction produces the precipitation of Al and transition metal hydroxides, cryptocrystalline SiO_2 and phosphates (Fig. 3). The precipitation of metal hydroxides and cryptocrystalline SiO_2 does not induce YLn fractionation in parent solution [47,48] because only weak surface complexation processes are involved. On the contrary, YLn have large affinity as regards of phosphates that usually accept in their lattice significant amounts of YLN with large preference for elements, from Sm to Gd, during crystallization of Ca-phosphate. The incorporation of intermediate REE induces REE fractionation in parent solution of newly formed phosphates that consequently assume specular REE features [49]. Similarly, if YLn-phosphate co-precipitate as solid solution of YLn, similar YLn behavior is recognized [42,43].

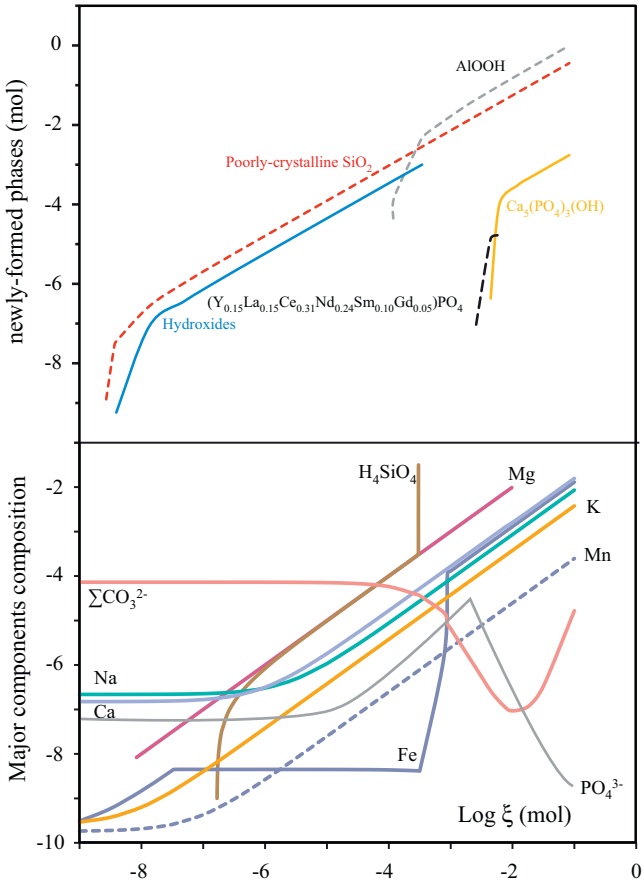

Fig. 3. Cumulative moles of newly-formed precipitates during SMLF–glass interaction. The simulations carried out considering glass–ash as the solid reactant and YLn as the special reactant indicate that AlOOH, hydroxides and poorly crystalline SiO_2 are the first-formed and the most abundant secondary minerals along the reaction path.

4. Implications

The combination of analytical results and model calculations that we present in this study gives a viable explanation for the occurrence of dendriform pulmonary ossification, a rare pulmonary pathology affecting people exposed to inhalation of YLn-bearing dust. DPO causes the development of branching bony spicules in the lung parenchyma of people with pulmonary fibrosis that, in the light of results of this study, can be explained as a consequence of the co-precipitation of YLn-phosphates from YLn-rich lung fluids due to dissolution of atmospheric particles.

We observe a strong similarity between $\log\{[YLn_i]/[YLn_i]_0\}$ patterns of BALs and those produced by co-precipitation of phosphates from parent solution. Such similarity suggests that the amplitude of YLn fractionations in BAL can be used as proxy to investigate the effects of human exposure to inhalation of YLn-bearing atmospheric dust and can represent a tool to develop strategies for the prevention of DPO.

Due to the increasing utilization of YLn for agricultural and industrial applications, the measurement of YLn fractionation in lung fluid (through BAL) has the potential to be a viable tracer of human exposure to heavy fluxes of fine particulates enriched in heavy metals pollutants.

Acknowledgments

This work was financially supported by ICT-3E grant provided by the Italian C.I.P.E. We are indebted to Drs N. Crimi, C. Mastruzzo and P. Pistorio for sample collections and to Dr. L. Marini for useful suggestions during thermodynamic modelling. We thank Prof. Wanida Jinsart and two anonymous reviewers for suggestions that improved the clarity of the manuscript. This paper reports scientific results belonging to the PhD project of L.A. Randazzo.

References

[1] N. Sakai, Medical mineralogy geochemistry: an interfacial sciences, Elements 3 (2007) 381–384.
[2] J.A. Baddini Martinez, S.G. Ramos, Inhalation of hydrocarbon combustion products as a cause of dendriform pulmonary ossification, Med. Hypotheses 71 (2008) 981–982.
[3] J.B. Pracyk, S.G. Simonson, S.L. Young, A.J. Ghio, V.L. Roggli, C.A. Piantadosi, Alveolar microlithiasis, Respiration 63 (1996) 254–260.
[4] H.K. Yoon, H.S. Moon, S.H. Park, J.S. Song, Y. Lim, N. Kohyama, Dendriform pulmonary ossification in patient with rare earth pneumoconiosis, Thorax 60 (2005) 701–703.
[5] R.W. Joines, V.L. Roggli, Dendriform pulmonary ossification. Report of two cases with unique findings, Am. J. Clin. Pathol. 91 (1989) 398–402.
[6] E. Sabbioni, R. Pietra, P. Gaglione, G. Vocaturo, F. Colombo, M. Zanoni, F. Rodi, Long-term occupational risk of rare-earth pneumoconiosis. A case report as investigated by neutron activation analysis, Sci. Total Environ. 26 (1982) 19–32.
[7] G. Vocaturo, F. Colombo, M. Zanoni, F. Rodi, E. Sabbioni, R. Pietra, Human exposure to heavy metals. Rare earth pneumoconiosis in occupational workers, Chest 83 (1983) 780–783.
[8] F. Sulotto, C. Romana, A. Berra, G.C. Botta, G.F. Rubino, E. Sabbioni, R. Pietra, Rare-earth pneumoconiosis: a new case, Am. J. Ind. Med. 9 (1986) 567–575.
[9] M. Takaya, Y. Shinohara, F. Serita, M. Ono-Ogasawara, N. Otaki, T. Toya, Dissolution of functional materials and rare earth oxides into pseudo alveolar fluid, Ind. Health 44 (2006) 639–644.
[10] J.W. McDonald, A.J. Ghio, C.E. Sheehan, P.F. Bernhardt, V.L. Roggli, Rare earth (cerium oxide) pneumoconiosis: analytical scanning electron microscopy and literature review, Mod. Pathol. 8 (1995) 859–865.
[11] S. Hirano, K.T. Suzuki, Exposure metabolism, and toxicity of rare earths and related compounds, Environ. Health Perspect. 104 (1996) 85–95.
[12] K. Luoto, M. Holopainen, J. Kangas, P. Kalliokoski, K. Savolainen, Dissolution of short and long rockwool and glasswool fibers by macrophages in flow through cell culture, Environ. Res. 78 (1998) 25–37.
[13] S. Forde, M.J. Hynes, B. Johnson, Dissolution of glass compositions containing no added lead in simulated lung fluid, Int. J. Hyg. Environ. Health 211 (2008) 357–366.
[14] K. Dias Da Cunha, M. Santos, F. Zouain, L. Carneiro, G. Pitassi, C. Lima, C.V. Barros Leite, K.C.P. Dália, Dissolution factors of Ta, Th, and U oxides present in pyrochlore, Water Air Soil Pollut. (2009) 1–7.
[15] K. Midander, I.O. Wallinder, C. Leygraf, In vitro studies of copper release from powder particles in synthetic biological media, Environ. Pollut. 145 (2007) 51–59.
[16] S. Scollo, P. Delcarlo, M. Coltelli, Tephra fallout of 2001 Etna flank eruption: analysis of the deposit and plume dispersion, J. Volcanol. Geotherm. Res. 160 (2007) 147–164.
[17] N. Oskarsson, The interaction between volcanic gases and tephra: fluorine adhering to tephra of the 1970 Hekla eruption, J. Volcanol. Geotherm. Res. 8 (1980) 16–23.
[18] P. Frogner, S.R. Gislason, N. Oskarsson, Fertilizing potential of volcanic ash in ocean surface water, Geology 29 (2001) 487–490.
[19] P. Delmelle, M. Lambert, Y. Dufrêne, P. Gerin, N. Óskarsson, Gas/aerosol-ash interaction in volcanic plumes: new insights from surface analyses of fine ash particles, Earth Planet. Sci. Lett. 259 (2007) 159–170.
[20] J. Taddeucci, M. Pompilio, P. Scarlato, Conduit processes during the July–August 2001 explosive activity of Mt. Etna (Italy): inferences from glass chemistry and crystal size distribution of ash particles, J. Volcanol. Geotherm. Res. 137 (2004) 33–54.
[21] M. Viccaro, C. Ferlito, L. Cortesogno, R. Cristofolini, L. Gaggero, Magma mixing during the 2001 event at Mount Etna (Italy): effects on the eruptive dynamics, J. Volcanol. Geotherm. Res. 149 (2006) 139–159.
[22] P. Censi, M. Sprovieri, D. Larocca, P. Aricò, F. Saiano, S. Mazzola, P. Ferla, Alteration effects of volcanic ash in seawater: anomalous Y/Ho ratios in coastal waters of the Central Mediterranean sea, Geochim. Cosmochim. Acta 71 (2007) 5405–5422.
[23] E. Bargagli, C. Bigliazzi, A. Leonini, N. Nikiforakis, M.G. Perari, P. Rottoli, Tryptase concentrations in bronchoalveolar lavage from patients with chronic eosinophilic pneumonia, Clin. Sci. 108 (2005) 273–276.
[24] EPA, Water Research Centre Procedure for the Determination of LC and LD (and ISO/IUPAC determination of LQ) (2005).
[25] S.A. Wood, A.E. Taunton, C. Normand, M.E. Gunter, Mineral-fluid interaction in the lungs: insights from reaction-path modeling, Inhal. Toxicol. 18 (2006) 975–984.
[26] E.R. Sholkovitz, Chemical evolution of rare earth elements: fractionation between colloidal and solution phases of filtered river water, Earth Planet. Sci. Lett. 114 (1992) 77–84.
[27] E.R. Sholkovitz, The geochemistry of rare earth elements in the Amazon River Estuary, Geochim. Cosmochim. Acta 57 (1993) 2181–2190.

[28] T.J. Wolery, Calculation of chemical equilibrium between aqueous solutions and minerals: the EQ3/6 software package, Report UCRL-52658, Lawrence Livermore National Livermore, California (1979).
[29] T.J. Wolery, A Computer Program for Geochemical Aqueous Speciation-Solubility Calculations: Theoretical Manual, User's Guide, and Related Documentation (Version 7.0). Report UCRL-MA-110662 PT III. Lawrence Livermore National Laboratory, Livermore, California. (1992).
[30] T.J. Wolery, S.A. Daveler, EQ6, A Computer Program for Reaction Path Modeling of Aqueous Geochemical Systems: Theoretical Manual, User's Guide, and Related Documentation (version 7.0), Report UCRL-MA-110662 pt IV, Lawrence Livermore National Laboratory, Livermore, California (1992).
[31] M. Accornero, L. Marini, The Double Solid Reactant Method for modeling the release of trace elements from dissolving solid phases: I. Outline and limitations, Environ. Geol. 55 (2008) 1627–1635.
[32] H. Eyring, The activated complex in chemical reactions, Chem. Rev. 17 (1935) 65–77.
[33] H. Eyring, The activated complex and the absolute rate of chemical reactions, J. Chem. Phys. 3 (3) (1935) 107–115.
[34] S.R. Gislason, E.H. Oelkers, Mechanism, rates, and consequences of basaltic glass dissolution: II. An experimental study of the dissolution rates of basaltic glass as a function of pH and temperature, Geochim. Cosmochim. Acta 67 (2003) 3817–3832.
[35] I. Prigogine, Introduction to Thermodynamics of Irreversible Processes, Wiley, New York, 1955.
[36] H.C. Helgeson, Evaluation of irreversible reactions in geochemical processes involving minerals and aqueous solutions-I. Thermodynamic relations, Geochim. Cosmochim. Acta 32 (1968) 853–877.
[37] K. Denbigh, The Principles of Chemical Equilibrium, 3rd ed., Cambridge University Press, 1971.
[38] P.J. Baxter, R. Dupree, V.L. Hards, S.C. Kohn, M.D. Murphy, A. Nichols, R.A. Nicholson, G. Norton, A. Searl, R.S.J. Sparks, B.P. Vickers, Cristobalite in volcanic ash of the Soufriere Hills Volcano, Montserrat, British West Indies, Science 283 (1999) 1142–1145.
[39] D. Wolff-Boenisch, S.R. Gislason, E.H. Oelkers, C.V. Putnis, The dissolution rates of natural glasses as a function of their composition at pH 4 and 10.6 and temperatures from 25 to 74 °C, Geochim. Cosmochim. Acta 68 (2004) 4843–4858.
[40] P. Dellino, D. Mele, R. Bonasia, G. Braia, L. La Volpe, R. Sulpizio, The analysis of the influence of pumice shape on its terminal velocity, Geophys. Res. Lett. 32 (2005) 1–4.
[41] O. Ersoy, Surface area and volume measurements of volcanic ash particles by SEM stereoscopic imaging, J. Volcanol. Geotherm. Res. 190 (2010) 290–296.
[42] R. Byrne, K. Kim, Rare earth precipitation and co-precipitation behavior: the limiting role of PO_4^{3-} on dissolved rare earth concentrations in seawater, Geochim. Cosmochim. Acta 57 (1993) 519–526.
[43] R. Byrne, X. Liu, J. Schijf, The influence of phosphate co-precipitation on rare earth distributions in natural waters, Geochim. Cosmochim. Acta 60 (1996) 3341–3346.
[44] W.P. Nash, Phosphate minerals in terrestrial igneos and metamorphic rocks, in: J.O. Nriagu, P.B. Moore (Eds.), Phosphate Minerals, Springer-Verlag, 1984, pp. 215–241.
[45] C.I. Grainger, L.L. Greenwell, G.P. Martin, B. Forbes, Eur. J. Pharm. Biopharm. 71 (2009) 318–324.
[46] P. Kulkarni, S. Chellam, M.P. Fraser, Tracking petroleum refinery emission events using lanthanum and lanthanides as elemental markers for PM2.5, Environ. Sci. Technol. 41 (2007) 6748–6754.
[47] F. Coppin, G. Berger, A. Bauer, S. Castet, M. Loubet, Sorption of lanthanides on smectite and kaolinite, Chem. Geol. 182 (2002) 57–68.
[48] K.A. Quinn, R.H. Byrne, J. Schijf, Comparative scavenging of yttrium and the rare earth elements in seawater: competitive influences of solution and surface chemistry, Aquat. Geochem. 10 (2004) 59–80.
[49] R.E. Hannigan, E.R. Sholkovitz, The development of middle rare earth element enrichments in freshwaters: weathering of phosphate minerals, Chem. Geol. 175 (2001) 495.
[50] Aiuppa, G. Dongarrà, M. Valenza, C. Federico, G. Pecoraino, Degassing of trace volatile metals during the 2001 eruption of Etna, in: A. Robock, C. Oppemheimer (Eds.), Volcanism and the Earth's Atmosphere Geophysical Monograph 139, American Geoph Union, Washinghton DC, 2003, pp. 41–54.